Dynamic Stability Analysis of Isolated Power System

Ramūnas Deltuva *[ID], Robertas Lukočius [ID] and Konstantinas Otas

Department of Electrical Power Systems, Faculty of Electrical and Electronics Engineering, Kaunas University of Technology, LT-51367 Kaunas, Lithuania; robertas.lukocius@ktu.lt (R.L.); konstantinas.otas@ktu.lt (K.O.)
* Correspondence: ramunas.deltuva@gmail.com; Tel.: +370-612-98623

Abstract: The islanded mode of operation of an electric power system (EPS) that has generation capabilities provided by conventional thermal power plants, by a pumped-storage power station, or from an interlink with a neighboring electric power system through an HVDC BtB converter is addressed in this paper. The risk for electrical power systems to fall into an islanded mode has recently grown, as it is caused not just by technical reasons but by a geopolitical situation as well. The current strains demand the close consideration of problems related to EPS operation in an islanded mode. This paper considers several. The research covers the following issues. The response of the islanded system to a sudden and spasmodic load change is analyzed in cases when the system deals with the disturbance with internal resources alone and with the help of an HVDC BtB converter's frequency control functionality. Analysis of the impact of the settings of the HVDC BtB converter on the system's response to disturbances is presented and the optimal set of parameters found. The impact of the system's extended inertia on the system's response is evaluated by using an additional unit of the pumped-storage power station in synchronous condenser mode. Transients in the system when switching a unit operating in synchronous condenser mode on and off are analyzed. The capability of the system to withstand major disturbances, such as disconnection of the pumped-storage power station's unit operating in a pump mode and disconnection of the HVDC BtB converter in emergency modes, if a situation demands, is researched. The research is carried out by numerical simulations using PSS Sincal Electricity Basic software. Updated operating parameters of the isolated power system and the LCC HVDC BtB converter, as well as frequency control automation provided by ABB, were used in the simulations.

Keywords: power system stability; isolated power system; HVDC BtB converter; filter; frequency deviation; dead-band; inertia

1. Introduction

In the changing geopolitical, economic, and diplomatic energy situation, each energy system must be able to maintain and ensure stability of the functioning of energy resources in critical conditions. Competences and ability to work independently of other energy systems must be strengthened in each electricity system.

The structure of an isolated energy system consists of electricity sources, equipment, their protection and automation, and load. All system elements must ensure reliable and stable operation of the electrical power system [1–4].

In the event of a disturbance or system failure, any EPS can be divided into separate and self-contained parts—islands. A distributed or isolated electrical power system must ensure energy reliability, stability, and the ability to work in critical and extreme operating conditions [5–9].

The stability of an isolated energy system is a very important indicator of reliability and quality. When analyzing the dynamic stability of an isolated EPS, it is necessary to assess whether the system will operate under extreme conditions for a short time or continuously. One of the key indicators of the dynamic stability of an EPS is the behavior of the generators under different network operating modes. Another very important point is the primary

and secondary power control of the generators. Finally, it is also important to consider the possibilities of using the operating functions of the HVDC BtB converter [10–12].

This article describes research and develops mathematical models for the analysis of an isolated energy system. This analysis is based on and supplemented by previous calculations and experiments. The developed models can be used as a basis to analyze the dynamic stability of an isolated energy system. These numerical models combine the authors' experiences and scientific achievements in dynamic stability research [12,13].

Attention has mainly been paid to the application of primary and secondary frequency and the active and reactive power control functions in numerical models. The applicability of voltage control and HVDC BtB converter operation functions is especially relevant in the models. Depending on the complexity of the dynamic model, these features can be adapted to a variety of isolated EPS operating modes. All dynamic models are designed for symmetric EPS operation. The focus has been on frequency and inertia management and control of the isolated EPS. The influence of the different operating modes of the HVDC BtB converter on the stability of the isolated energy system is also very important [2–10].

This paper is organized as follows. Section 2 describes the structure and the main parameters of the analyzed isolated power system. Analysis of the system's frequency dependence on a rapid load change is presented in Section 3. Section 4 is dedicated to an analysis of the impact of the HVDC BtB converter's settings on the system's response to a disturbance. The response of the system to the switching of the synchronous condensers is analyzed in Section 5. Section 6 presents research on the system's response to a load change when the HVDC BtB converter's frequency control function is on. Emergency operating modes—disconnection of the unit operating in pump mode and HVDC BtB converter disconnection—are considered in Section 7. Finally, in Section 8, the results are summarized, and conclusions are presented.

2. Structure and Operating Conditions of the Researched Isolated EPS

The analyzed isolated electric power system consists of 330 kV open switchgear busbars, lines, and a switching apparatus, and autotransformers, power transformers, and 110 kV open switchgear busbars. The HVDC BtB converter is connected to the 330 kV grid and the 330 kV line.

The operating devices of the isolated EPS are:

- Generator G1 = 200 MW, operates through 330 kV switchgear;
- Synchronous condenser SC1 mode (−10 MW), operates through 330 kV switchgear;
- Synchronous condenser SC2 mode (−10 MW), operates through 330 kV switchgear;
- Motor P—pump mode (−220 MW), operates through 330 kV switchgear;
- Generator G2 = 200 MW, operates through 330 kV switchgear;
- Generator G3 = 180 MW, operates through 330 kV switchgear;
- Generator G4 = 120 MW, operates through 110 kV switchgear;
- Generator G5 = 100 MW, operates through 110 kV switchgear;
- HVDC BtB converter (−225 MW) exports from the islanded EPS to the neighboring EPS and operates through 330 kV switchgear.

The scheme of the isolated power system is presented in Figure 1.

During simulation, it is assumed that the operating conditions of the EPS are:

1. Active power generation capability of the isolated system is 800 MW;
2. One unit (case A) and two units (case B) are operating in SC (synchronous condenser) mode;
3. HVDC BtB converter operates in (−225 MW) export mode from the isolated EPS to the neighboring EPS.

The structure of the model design of the frequency and damping controller is shown in Figure 2.
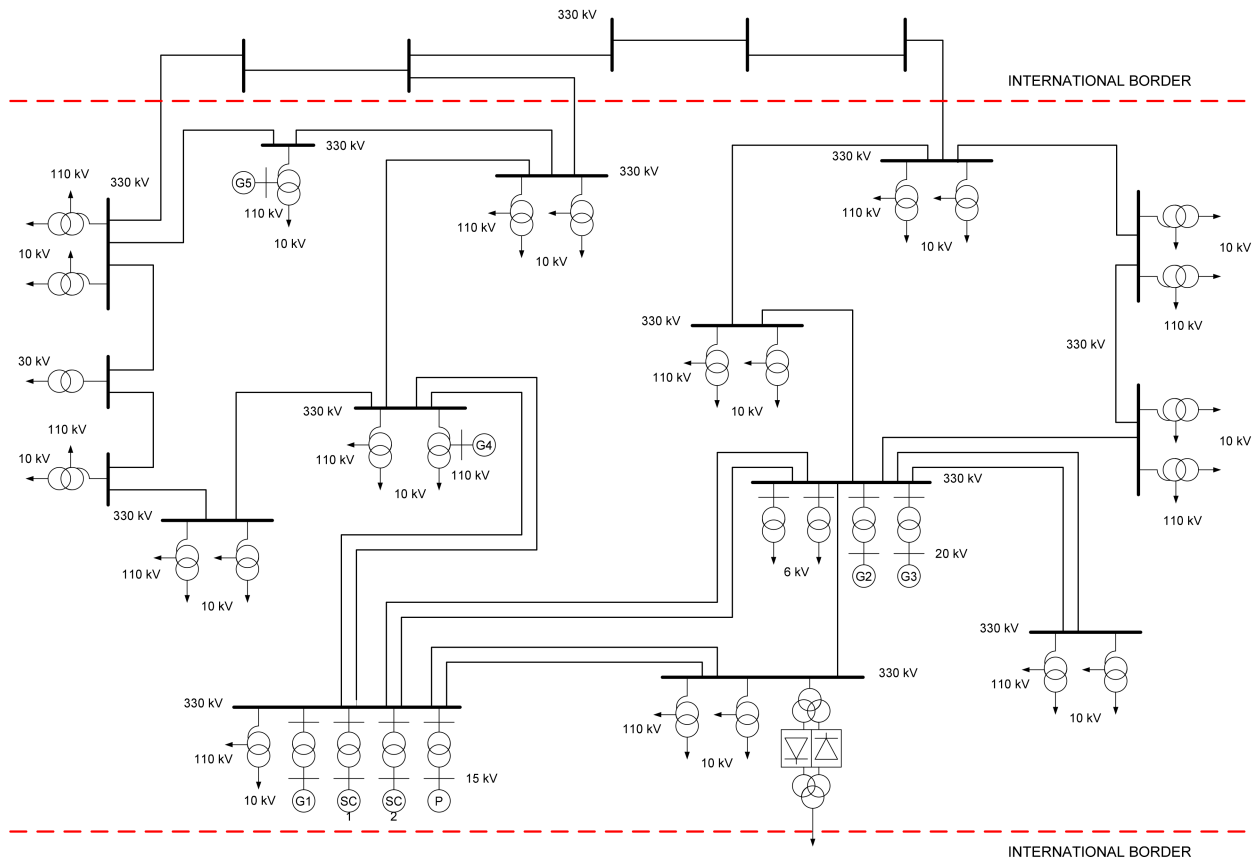
Figure 1. Isolated power system scheme.
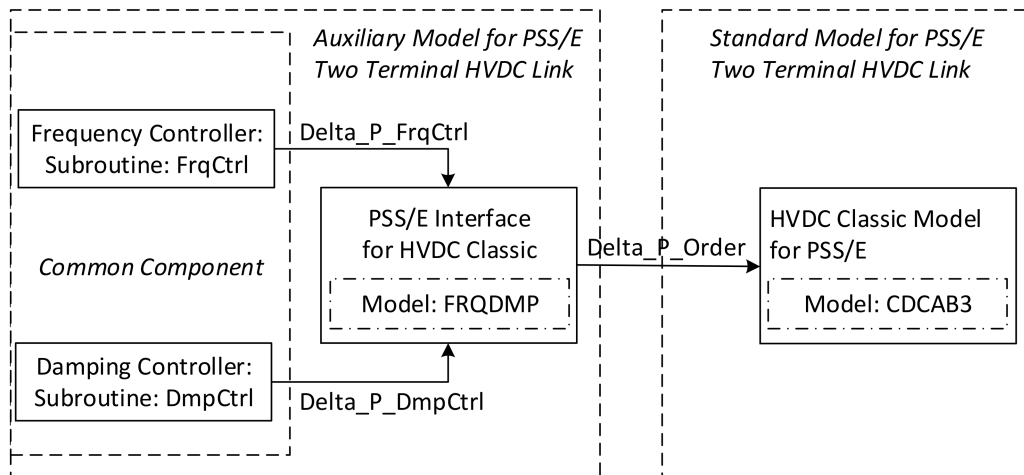
Figure 2. Structure of the model design of the frequency and damping controller.

A two-terminal DC model with a frequency controller model was added in the *dyr* file to model the dynamic aspects of the HVDC. A FRQDMP model summarizes the power modulation from the frequency controller and then sends the modulation signal to a standard classic model CDCAB3 to implement the power.

An HVDC transmission system can be used to support the frequency of a disturbed power system (due to loss of generation or large loads or sections of the system) by adjusting the power taken from the other (healthy or supporting) system connected to the HVDC transmission system. Thus, one system that supports the other will have its frequency

changed. A large system can easily support a small system, while in the case of similar sizes of system capacity, this influence needs to be considered.

The frequency controller is designed in such a way that its preference is to retain frequency limits in the healthy (primarily undisturbed) system. The frequency controller principle is thus to assist with balancing the power loss/change between the systems and still reduce the impact on the healthy system in order to avoid deviations beyond its frequency limits.

When the frequency of the faulty (primarily disturbed) system exceeds any of the dead-band limits, it will activate a power order change (ΔP_{DC}) to the converters to reduce the frequency deviation. The HVDC link will adjust the power to control the frequency in the faulty AC grid.

As a result, the frequency of the healthy system will also be changed. If its frequency also exceeds any of the dead-band limits, it will activate a power order to reduce (counteract) the initial change (ΔP_{DC}) to the converters in order to reduce its frequency deviation. The frequency controller uses information about the frequency in both grids. Consequently, the operation of the frequency controller requires communication between the rectifier and the inverter of the HVDC link.

This frequency controller is designed for certain worst-case conditions, where EPSs are islanded from the rest of the network. It gives a delta power contribution to the Active Power Controller (APC) in proportion to the frequency deviation, as shown in Figure 3. The controller has a transfer function with a low pass characteristic with a dead-band on the input signal and a limiting function on the output signal.
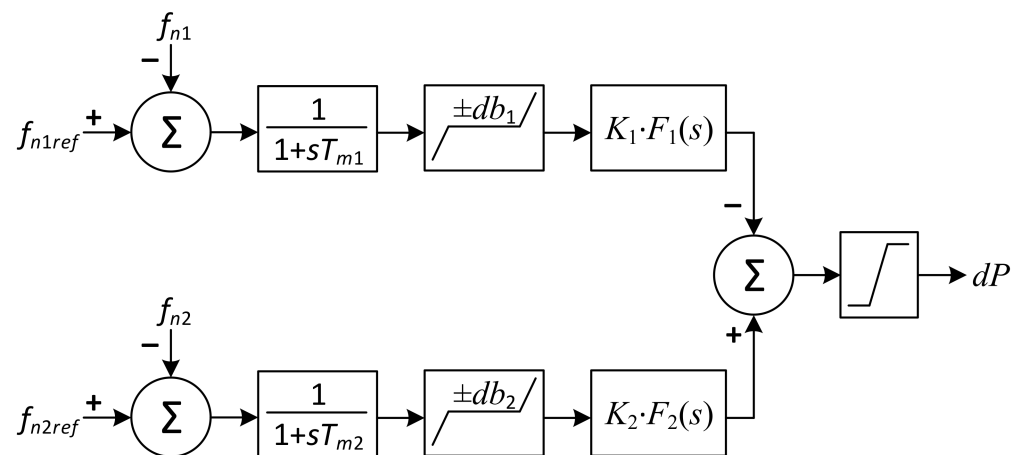
Figure 3. Structure of a frequency controller.

The frequency of each region is measured and compared with the reference frequency of the respective region to obtain the frequency error. f_{n1} and f_{n2} above refer to the frequency of networks 1 (rectifier system) and 2 (inverter system), respectively. For a reverse power operation, the polarities should change. The resulting signals are then passed through a dead-band of 0.01 Hz and then an amplifier with gain set to 2500 MW per Hz corresponding to 0.4% droop characteristics. It is only possible to activate frequency control from one AC network at a time. If a frequency controller is activated in the isolated EPS region for a power flow direction from the isolated EPS, an increase in frequency in the isolated EPS region should be counteracted by an increase in power flow and vice versa. The incremental (or decremental) change in power order is separately generated as per the operating frequency of each region and is applied to the pole controller, where they are summed together, along with the output of the power oscillation damping controller and the base power order. The following settings for the frequency controller have been defined in the study: $db = \pm 0.01$ Hz; $t_1 = 2$ s; gain $K = 2500$ MW/Hz.

The simulation time interval to be used is 5 ms, which is a suitable time interval when using the HVDC model. The need for the frequency controller is found to be negligible,

even when the normal load flows are subjected to the worst-case disturbances, such as large generation outages or sudden load losses in the system. However, in certain worst cases (such as where EPSs are islanded from the rest of the network), the criterion for designing the frequency controller is to utilize the full capacity of the HVDC BtB link to address the 0.2 Hz of frequency deviation that occurs in the isolated EPS AC network due to the load and generation unbalance created in the network.

G1, SC, P model: VGDS-1025/245/40UHL represents generator GI, which operates in Hydro-generator mode, Synchronous condenser mode, Motor pump mode, and does support the FFR function, but only when the hydro-generator has temporary droop settings and time constants. These settings are manually set. A mathematical model of generator G1's structure is shown in Figure 4.
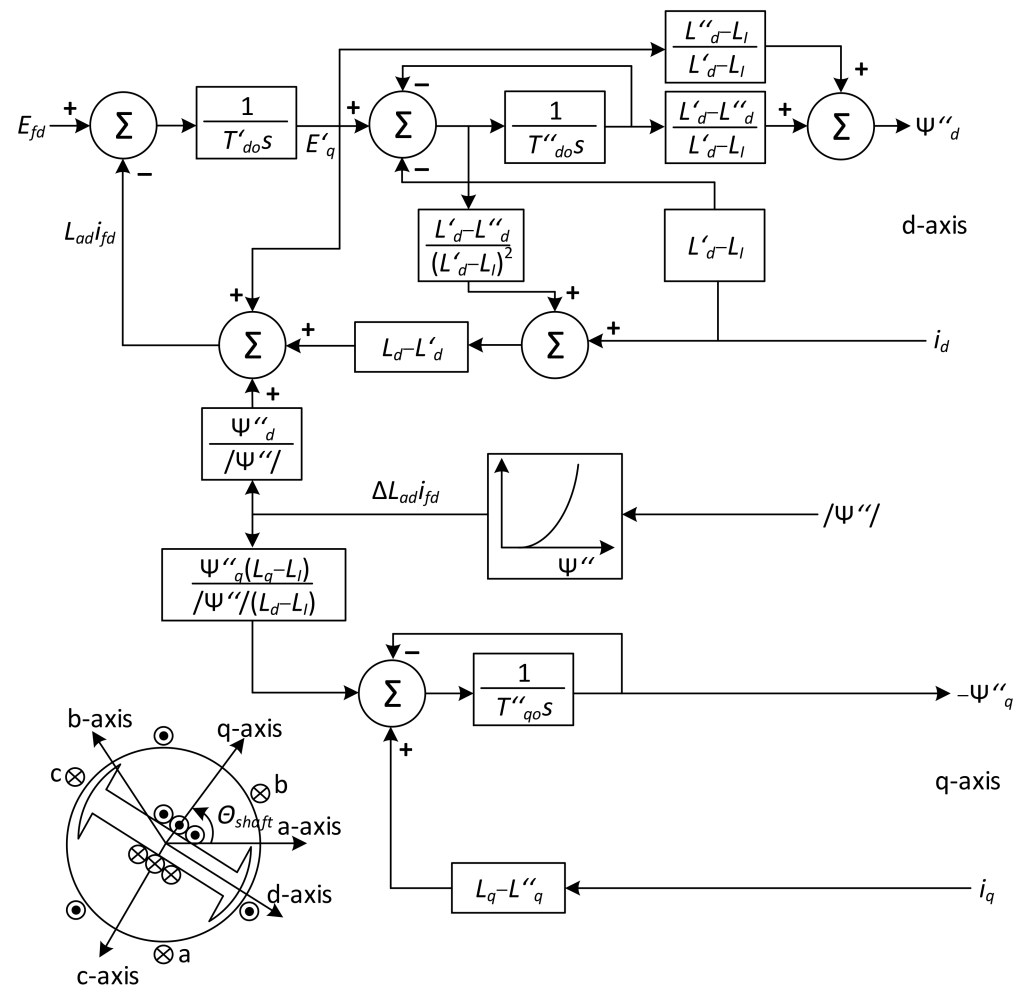
Figure 4. Structure of the electromagnetic model of a bright pole generator.

In this model, the evaluation of rotor magnetic saturation occurs in the direct-axis d and in the quadrature-axis q. Saturation is described by a quadratic function. The model assumes that the magnetization acts on all of the generator's existing mutual and leakage inductances. In modeling, the saturation value is considered to depend on both the rotor (excitation) and the stator currents [14]. Therefore, the effective values of the generator parameters in the model at each moment are converted from:

1. Unsaturated values of all of the generator's reactive resistances;
2. Instantaneous values of the coupled magnetic flux.

The G1 parameters are shown in Table 1.

Table 1. Hydro-generator G1's main parameters.

Name	Marking	Measurement	G1
Apparent power	S_N	MVA	248
Active power	P_N	MW	225
Nominal voltage	U_N	kV	15.75
Power factor	$cos\,(\varphi)$	p.u.	0.85
Number of pole pairs	p	-	20
Rotation speed	s	rot/min.	150
Zero phase-sequence impedance	X_0	p.u.	0.05–0.19
Negative phase-sequence impedance	X_2	p.u.	0.38
Coupling	-	-	star grounded through transformer
Direct-axis synchronous reactance	X_d	p.u.	1.42
Quadrature-axis synchronous reactance	X_q	p.u.	0.96
Direct-axis transient reactance	X_d'	p.u.	0.45
Direct-axis sub-transient reactance	X_d''	p.u.	0.32
Quadrature-axis sub-transient reactance	X_q''	p.u.	0.32
Stator winding leakage reactance	X_1	p.u.	0.20
The value of the saturation function	S_1	-	0.11
Inertia	H	p.u.	4.0
Damping	D	p.u.	0.0
Direct-axis idle transient time constant	T_{d0}'	s	9.80
Direct-axis idle sub-transient time constant	T_{d0}''	s	0.10
Quadrature-axis idle transient time constant	T_{q0}'	s	0.15

The G2 model uses a combined cycle gas turbine and turbogenerator and does support the FFR function, but it works on limited value. The G3 model is a TVV-220-2 turbogenerator and does support the FFR function. The G4 model is a TVF-150-2UZ turbogenerator and does not support the FFR function. The G5 model is a TVF-120-2 turbogenerator that does support the FFR function. A mathematical model of the structure of generators G2–G5 is shown in Figure 5.

This model assumes that saturation affects both the direct-axis and quadrature-axis inductive resistances, and that the mutual inductances vary with the bounded magnetic flux generated beyond the transient inductive resistance [14].

The parameters for G2–G5 are shown in Table 2.

Table 2. Main parameters of turbogenerators G2–G5.

Name	Marking	Measurement	G2	G3	G4	G5
Apparent power	S_N	MVA	524	220	150	120
Active power	P_N	MW	445	180	120	100
Nominal voltage	U_N	kV	19	20	10.5	10.5
Power factor	$cos\,(\varphi)$	p.u.	0.85	0.82	0.8	0.8
Number of pole pairs	p	-	1	1	1	1
Rotation speed	s	rot/min.	3000	3000	3000	3000
Zero phase-sequence impedance	X_0	p.u.	0.13	0.088	0.10	0.10
Negative phase-sequence impedance	X_2	p.u.	0.24	0.21	0.23	0.23
Coupling	-	-	star	double star	double star	double star
Direct-axis synchronous reactance	X_d	p.u.	2.0	1.70	1.90	1.90
Quadrature-axis synchronous reactance	X_q	p.u.	1.92	1.61	1.80	1.65
Direct-axis transient reactance	X_d'	p.u.	0.29	0.26	0.28	0.25
Direct-axis sub-transient reactance	X_d''	p.u.	0.24	0.17	0.18	0.19
Quadrature-axis transient reactance	X_q'	p.u.	0.48	0.48	0.45	0.52
Stator winding leakage reactance	X_1	p.u.	0.19	0.15	0.15	0.10
The value of the saturation function	S_1	-	0.036	0.059	0.19	0.18
Inertia	H	p.u.	5.78	2.70	3.40	3.15
Damping	D	p.u.	0.0	0.0	0.0	0.0
Direct-axis idle transient time constant	T_{d0}'	s	6.70	5.90	6.45	7.50
Direct-axis idle sub-transient time constant	T_{d0}''	s	0.04	0.17	0.17	0.06
Quadrature-axis idle transient time constant	T_{q0}'	s	0.60	0.85	0.85	2.08
Quadrature-axis idle sub-transient time constant	T_{q0}''	s	0.08	0.15	0.15	0.05
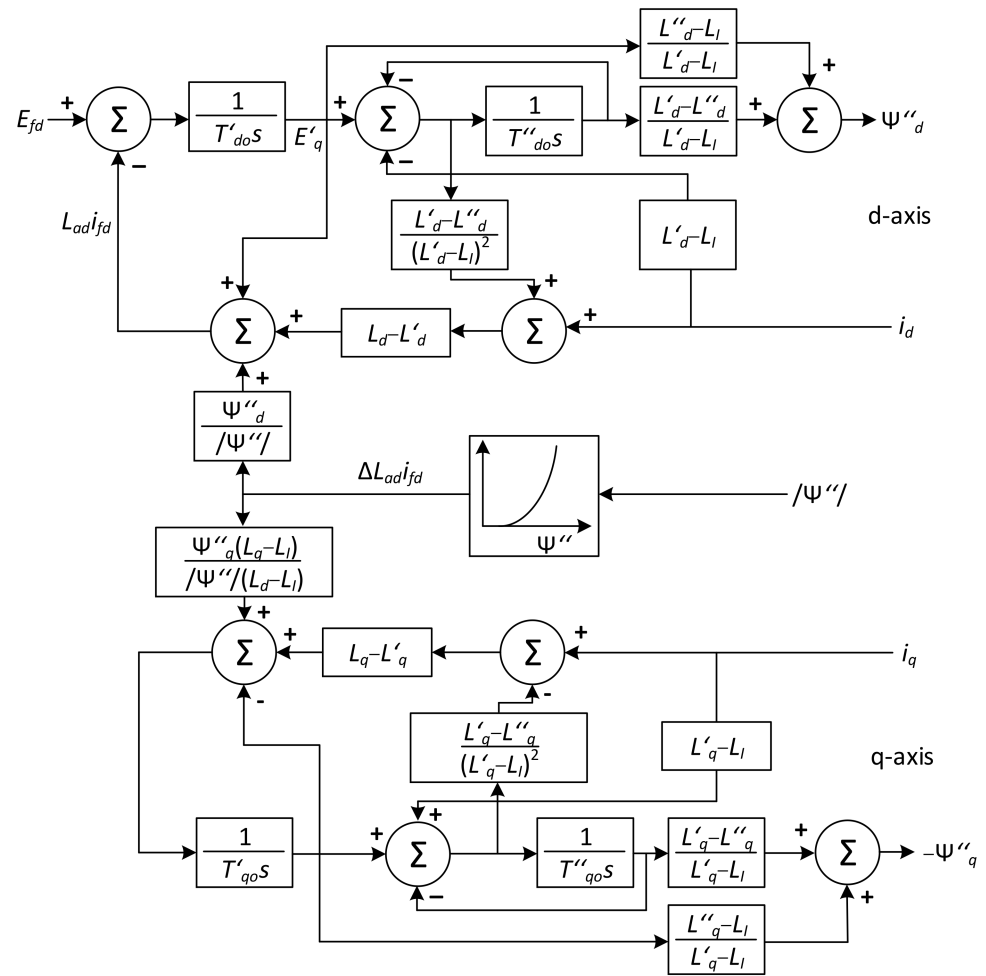
Figure 5. Structure of the electromagnetic model of a blurred generator.

3. Response of the Isolated EPS to a Load Change

In this section, the response of the isolated system to load increase and decrease is analyzed, and the amounts of load change determining frequency drops in the system to critical values are found. The impact of the system's additional inertia, determined by the connection of an additional unit operating in SC mode, is evaluated. The analysis is performed for a case in which the frequency control function of the HVDC BtB is turned off.

3.1. Response of Isolated EPS to a Load Increase

Analysis of the dependence of a frequency drop in the system on an increase in load is accomplished by simulating a soaring change of the transmitted active power flow through the HVDC BtB from 10 to 50 MW, in 10 MW increments. During the simulation, it was considered that only one unit operated in synchronous condenser mode (case A).

The simulation results are shown in Figure 6a,b.

The results show that, in cases with a load jump greater than 40 MW, damped active power oscillations occur. Damped active power oscillations are caused by a voltage drop in the 330 kV section. Fluctuations in the 330 kV voltage are caused by a decrease in the active power flow, i.e., due to the response of the system to a change in power. The dependence of the frequency drop on the active power change is presented in Table 3. A drop in frequency greater than short-term tolerance, i.e., >200 mHz, is reached in the event of the load increasing by 30 MW or more [15–19].

(**a**)   (**b**)
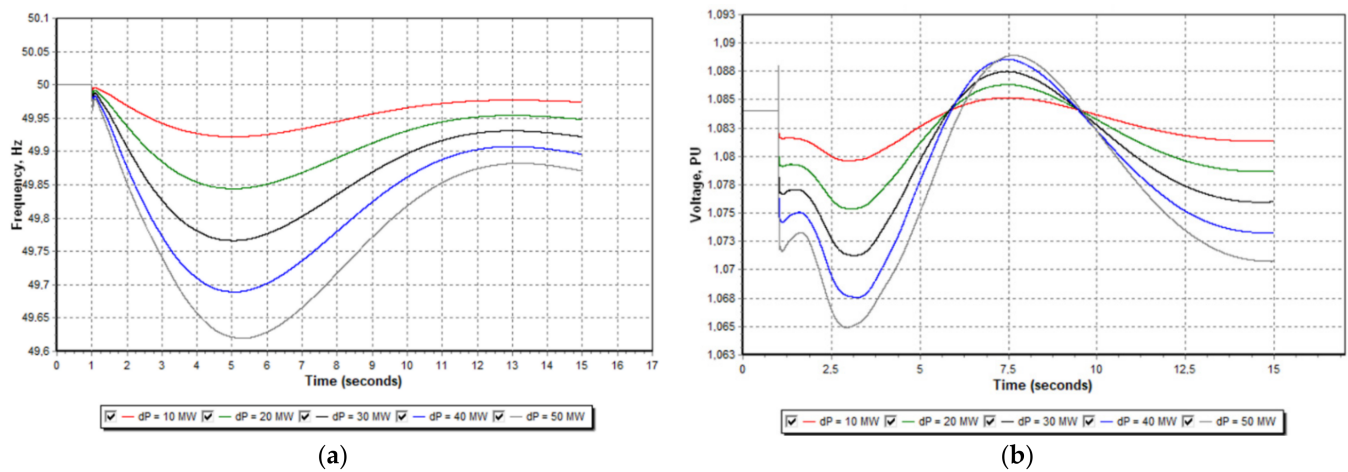
Figure 6. (**a**) Frequency change in the isolated power system caused by a load increase (case A). (**b**) Voltage fluctuations on the 330 kV side caused by a load increase (case A).

Table 3. Frequency change in the isolated power system.

Power Change, MW	Frequency, Hz	Power of HVDC Converter, MW
10	49.92	−235
20	49.83	−245
30	49.77	−255
40	49.69	−265
50	49.62	−275

A frequency drop to the critical, i.e., to 49.80 Hz, limit corresponds to the load increasing by 25 MW. The minus sign here (in Table 3) denotes active power export from the EPS.

After estimating the maximum allowable disturbance possible in the isolated EPS (30 MW) at the existing calculated inertia, the reaction of the EPS when two units are operating in the system in SC (synchronous condenser) mode was analyzed in Figure 7.
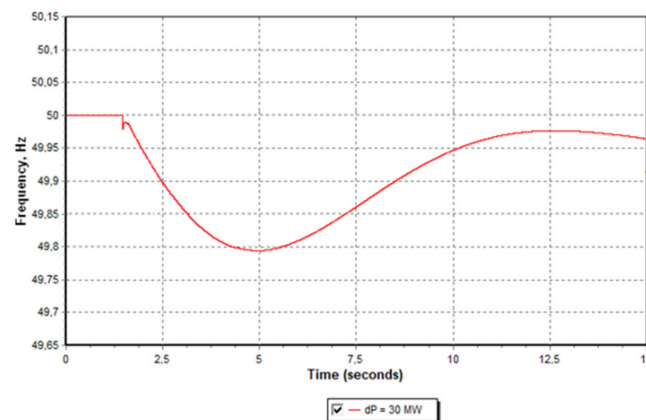
Figure 7. Frequency change in the isolated power system caused by a load increase (case B).

When two units operate in SC mode, with a disturbance of 30 MW, the frequency of the isolated EPS drops to 49.79 Hz. A frequency drop to the 49.80 Hz limit corresponds to the load increasing by 27.5 MW. The total inertia of an isolated EPS is equal to the sum of the inertias of all the generators operating in the system. All generators and units operating in pump mode and hydro-electric generators operating in SC (synchronous condenser) mode also contribute to the total inertia of an isolated EPS. Wind power plants and solar power plants do not provide additional inertia to an isolated EPS [15,20–23].

The amount of inertia required for the stable operation of an isolated EPS is equal to 25 MWs for every 1 MW imbalance. This amount of inertia ensures that the frequency of the isolated EPS will not drop to the critical value of 49.80 Hz [15–19].

The following conditions must be ensured in the isolated EPS [16–19,24]:

1. The maximum generation source in an isolated EPS shall not exceed 200 MW;
2. Emergency power control of the HVDC BtB converter is enabled (HVDC EPC).

The amount of inertia required for the stable operation of an isolated EPS is equal to 5000 MWs. The inertia of an isolated EPS is 5793 + (SC1) 992 + (SC2) 992 MWs [15,21,22,25,26]. The inertia constant (H) of an isolated EPS operating with generators ranges between 2.5–6.0 [27–30].

Factor k of an isolated EPS is a relative value that indicates the response of the system (primary control, MW) to frequency deviations (Hz) and is expressed as follows:

$$k = \frac{\Delta P}{\Delta f} \tag{1}$$

where ΔP is active power change (MW), and Δf is frequency change (Hz).

Factor k helps to easily determine the amount of primary control of active power, as well as active power imbalance.

The value of factor k is determined by knowing the sum of P_N values of all generators operating in the isolated EPS with primary frequency control enabled:

$$k = \frac{\sum (P_{N\ FCR})}{2} \tag{2}$$

The k factor absolute value of a single power plant is:

$$k_{PP} = \frac{P_N}{f_N} \cdot \frac{1}{\delta} \tag{3}$$

where P_N is the nominal value of the active power of the generator, which is different for each generator, f_N is the nominal frequency of 50 Hz, and δ is droop relative value (%).

Then, the k factor absolute value of multiple power plant is:

$$k_{sum\ PP} = \sum_{1}^{i} \left(\frac{P_{N\ i}}{f_{N\ i}} \right) \cdot \left(\frac{1}{\delta_i} \right) \tag{4}$$

The total k factor value is equal to:

$$k_{total} = k_{sum\ PP} + k_{self\ regulation} \tag{5}$$

where $k_{self\ regulation}$ is the self-regulation k factor of a load, the frequency-dependent load value (MW/Hz).

Calculations of the factor k are useful:

1. With small frequency deviations (up to 0.2–0.25 Hz);
2. With the low dead-band of operating generators ($\geq$10 mHz);
3. When the power plants in operation have a sufficient reserve of active power;
4. When the EPS is in a quasi-static state (Δf varies up to 0.2–0.3 Hz).

Calculations of the factor k are performed only when the operation of the isolated EPS is stable.

In order to ensure the capability of an isolated EPS to operate independently, sufficient power reserves are needed to balance the isolated system and to perform frequency control [16–19,24].

The FCR (Frequency Containment Reserves) during normal EPS isolated operation should be = 1.1 $P_{max.infeed}$ (where $P_{max.infeed}$ is the biggest infeed in the EPS).

In a case where the dimensioning fault in the EPS during isolated operation is 200 MW, then in order to ensure stable frequency control during isolated operation, the amount of FCR in the EPS should be around ±220 MW.

It is expected that at least ca. ±50 MW of FCR is initially received from the neighboring transmission system operator (TSO) through the HVDC link. The rest of the needed FCR must be deployed locally by the isolated EPS. The FCR of the isolated EPS is 200 MW. The full activation time of the FCR is 30 s, and full activation causes frequency deviation (or ±200 mHz).

3.2. Response of Isolated EPS to a Load Decrease When HVDC BtB Converter's Frequency Control Function Is Off

A frequency increase in the isolated EPS is simulated by a soaring change of the active power flow through an HVDC BtB converter or with the operating generators of the system from 10 to 50 MW, in 10 MW increments. In the digital simulation, it was assumed that one unit (case A) was operating in SC (synchronous condenser mode). The simulation results are shown in Figure 8a,b.

(**a**)　　　　　　　　　　　　　　　　　　　　(**b**)
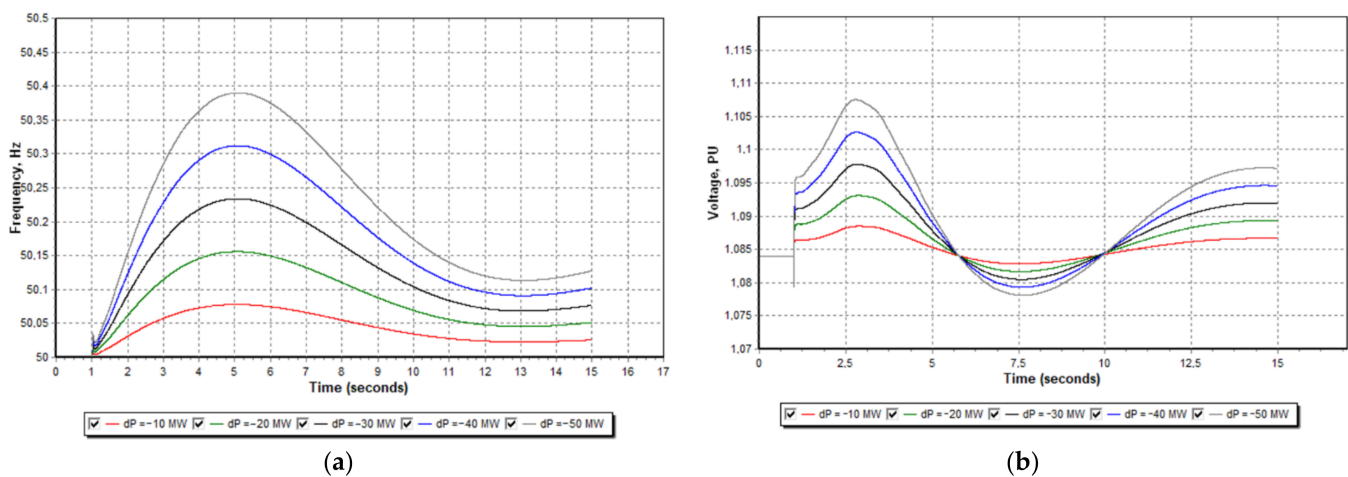
Figure 8. (**a**) Frequency change in the isolated power system caused by a load decrease (case A). (**b**) Voltage fluctuations on the 330 kV side caused by a load decrease (case A).

When changing the active power transmitted by the HVDC BtB converter, there are no oscillations in the active power. The short-term frequency tolerance of 200 mHz of the isolated EPS is reached only in the event of an increase in active power by 30 MW or more. Frequency increments up to 50.20 Hz correspond to the load decreasing by 25 MW. The minus sign here represents active power export from the EPS. The isolated power system frequency change values are given in Table 4 [16–19,24].

Table 4. Frequency change in the isolated power system.

Power Change, MW	Frequency, Hz	Power of HVDC Converter, MW
−10	50.08	−215
−20	50.17	−205
−30	50.23	−195
−40	50.31	−185
−50	50.39	−175

After estimating the maximum possible disturbance (30 MW) with a calculated inertia of 7777 MWs, the reaction of the isolated EPS when two (case B) SC (synchronous condenser) units are operating in the system was analyzed. The inertia of the isolated EPS is 5793 + (SC1) 992 + (SC2) 992 MWs [15,21,22,25,26]. The simulation results are shown in Figure 9.
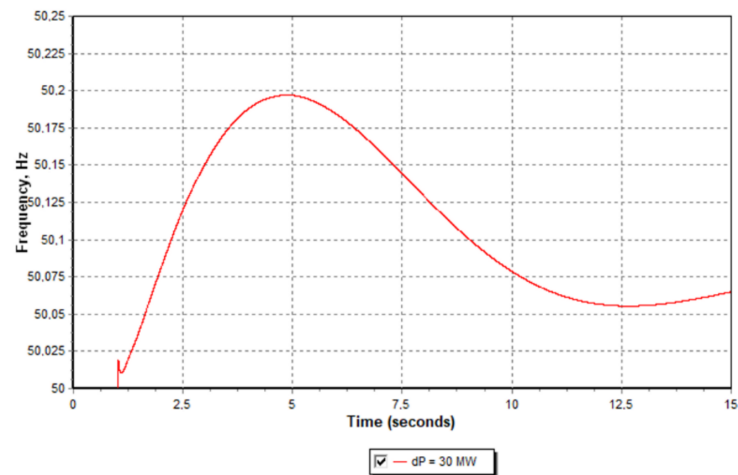
Figure 9. Frequency change in the isolated power system caused by a load decrease (case B).

When the two units are operating in an isolated EPS in SC (synchronous condenser mode) mode and with a 30 MW disturbance, the frequency of the system increases up to 50.19 Hz. A frequency rise to the critical, i.e., to 50.20 Hz, limit corresponds to the load decreasing by 31 MW.

4. Impact of the Isolated System's Response on Settings of HVDC BtB Converter

The influence of the HVDC BtB converter's settings on the isolated system's response is analyzed in this section. The impact of the converter's filters and settings of its gain factor K, ramp speed, and their combinations is considered.

4.1. Impact of HVDC BtB Converter Filters on Active Power Transmission

During the simulation, active power transmission was analyzed for the cases:

1. Without HVDC BtB converter filters;
2. With one HVDC BtB converter filter;
3. With two HVDC BtB converter filters.

The impact on active power transmission is examined by increasing the load of the HVDC BtB converter by 30 MW. The filters are of capacitive type, so their rated reactive power is 92 MVar. The simulation results are shown in Figure 10.
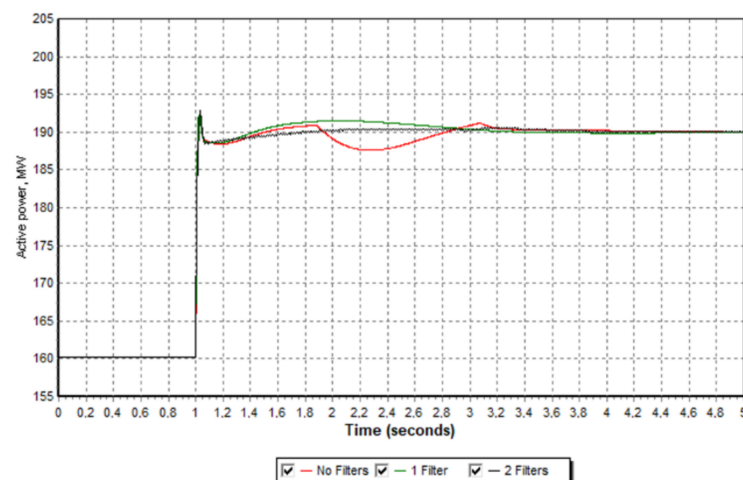
Figure 10. Influence of filters on the active power transfer of the HVDC BtB converter.

Analysis of the results showed that the HVDC BtB converter filters reduce active power oscillations in the presence of sudden changes in active power in the isolated EPS. Both harmonic filters must be kept on during operation of the isolated EPS.

4.2. Setting the Optimal Frequency Control Parameters for the HVDC BtB Converter

The optimal frequency controller parameters are found by changing the gain *K* and the power ramp speed parameters. In the numerical simulation, it was assumed that the load increased by 30 MW, i.e., the active power flow of the HVDC BtB converter was changed, and the dead-band was set to 50 mHz. After selecting the optimal parameters for the HVDC BtB converter, the digital simulation was performed with different frequency dead-band limits.

Simulations were performed with different values of gain factor *K* of the HVDC BtB converter, when: *K* = 100 MW/Hz, *K* = 1250 MW/Hz, *K* = 2500 MW/Hz, and the ramp speed of active power: 100 MW/s, 200 MW/s, 600 MW/s, 1000 MW/s.

The simulation results are shown in Figures 11 and 12.

(a)　　　　　　　　　　　　　　　　　　　　　　　(b)
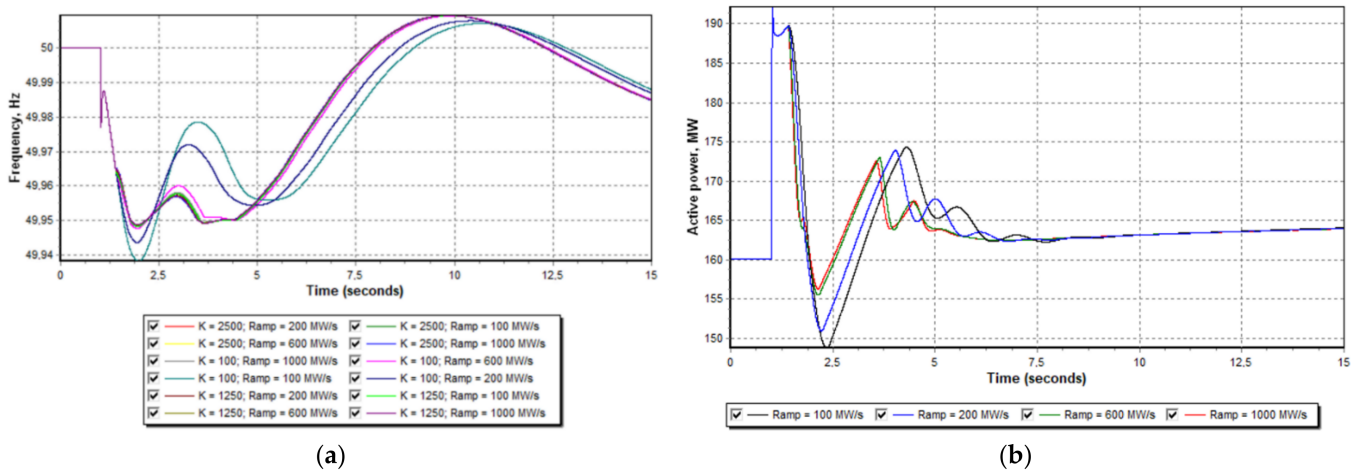
Figure 11. (**a**) Frequency dependence of the isolated power system on the frequency control parameters of the HVDC BtB converter. (**b**) The response of an active power to a load change when the gain is *K* = 100 MW/Hz.

(a)　　　　　　　　　　　　　　　　　　　　　　　(b)
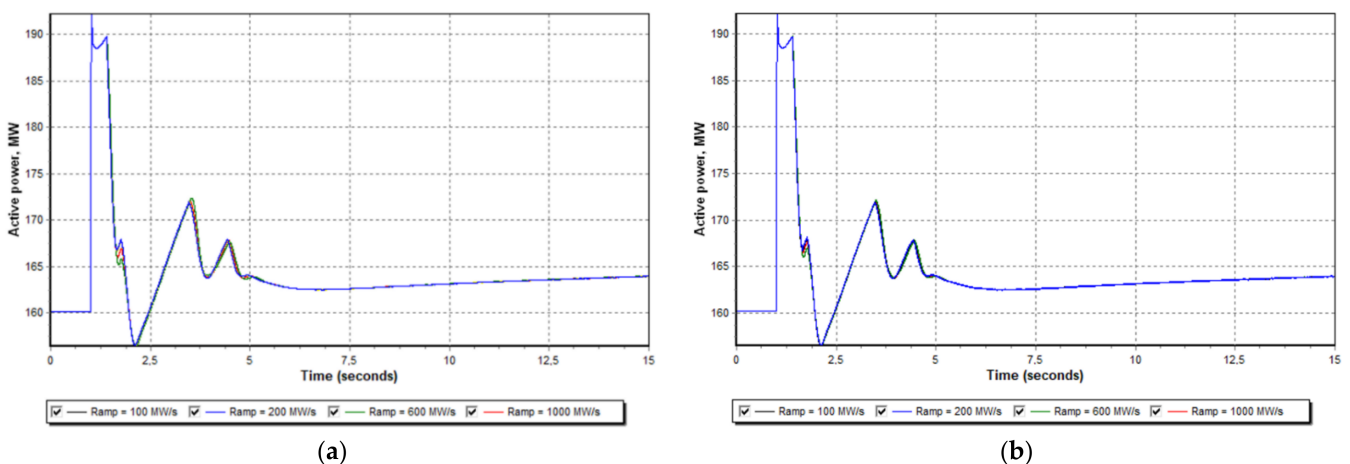
Figure 12. (**a**) The response of an active power to a load change when the gain is *K* = 1250 MW/Hz. (**b**) The response of an active power to a load change when the gain is *K* = 2500 MW/Hz.

Analysis of the obtained results revealed that all frequency control parameters of the HVDC BtB converter selected during the simulation can be used for the operation of the isolated EPS. A slower response is observed when the gain factor *K* = 100 MW/Hz and the

ramp speed of active power is 100 MW/s; then, the frequency of the isolated EPS drops to 49.93 Hz. When the ramp speed of active power is 200 MW/s, the frequency of the isolated EPS drops to 49.945 Hz [21,22,25,26,31–34].

5. Impact of the Isolated System's Response on Settings of HVDC BtB Converter

The response of the isolated power system to disconnection and to powering on the synchronous condenser for various system configurations is researched and analyzed in this section. The impacts of the HVDC BtB converter's frequency control function and its parameter settings, as well as the system's inertia improvement with an additionally connected synchronous condenser, are taken into consideration.

5.1. Response of Isolated EPS to SC Disconnection

The initial conditions for the digital simulation were as follows: 1. The operating SC (synchronous condenser) disconnects with (-10 MW) load; 2. SC frequency control gain is 1250 MW/Hz and corresponds to 0.8% droop; 3. SC frequency control gain is 250 MW/Hz and corresponds to 4% droop; 4. the ramp speed of active power is 100 MW/s; 5. the dead-band of the system's frequency change is 10 mHz, at a gain of $K = 1250$ MW/Hz; 6. SC reactive power is not transferred to the isolated EPS, and $Q = 0$ MVar. The simulation results are shown in Figures 13–16. FC here denotes Frequency Control.

(**a**)

(**b**)
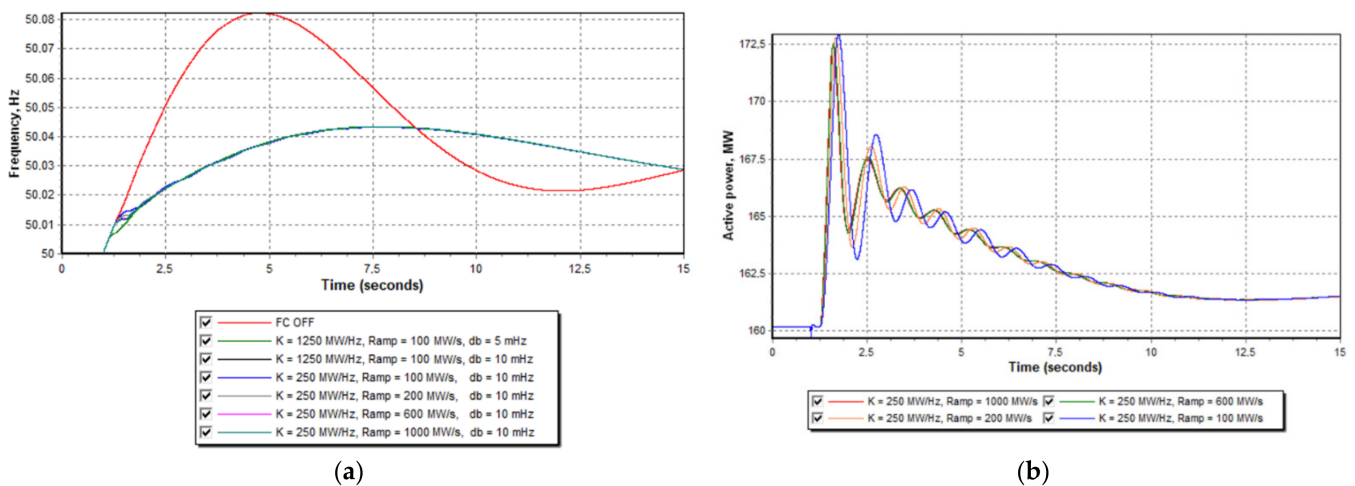
Figure 13. (**a**) Frequency change in the isolated power system—synchronous condenser disconnection. (**b**) Active power response of the HVDC BtB converter when $db = 10$ mHz.

(**a**)

(**b**)
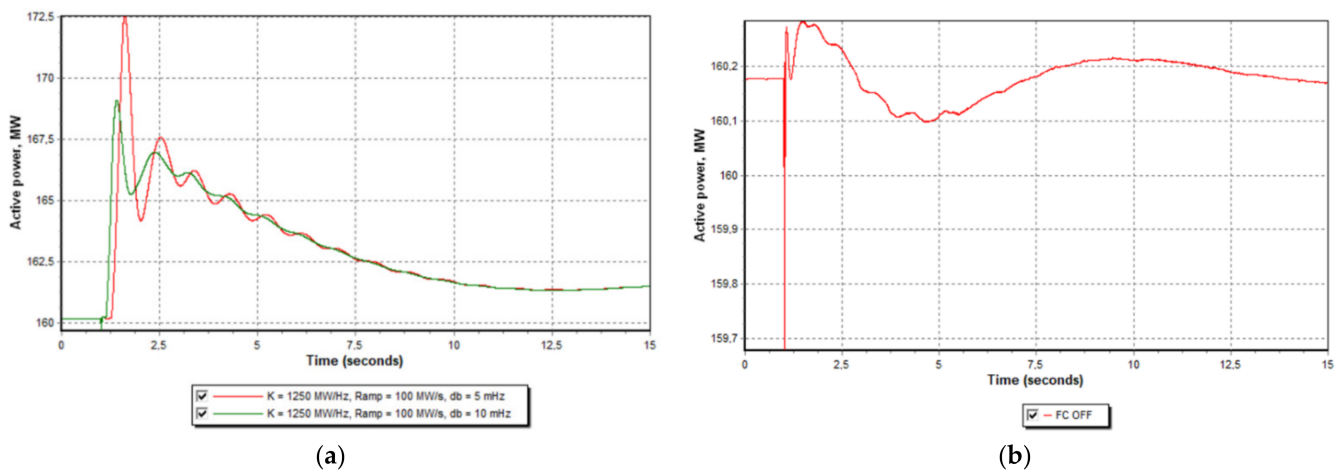
Figure 14. (**a**) Active power response of the HVDC BtB converter. (**b**) Reaction of the HVDC BtB converter when FC is off.

(a)
(b)
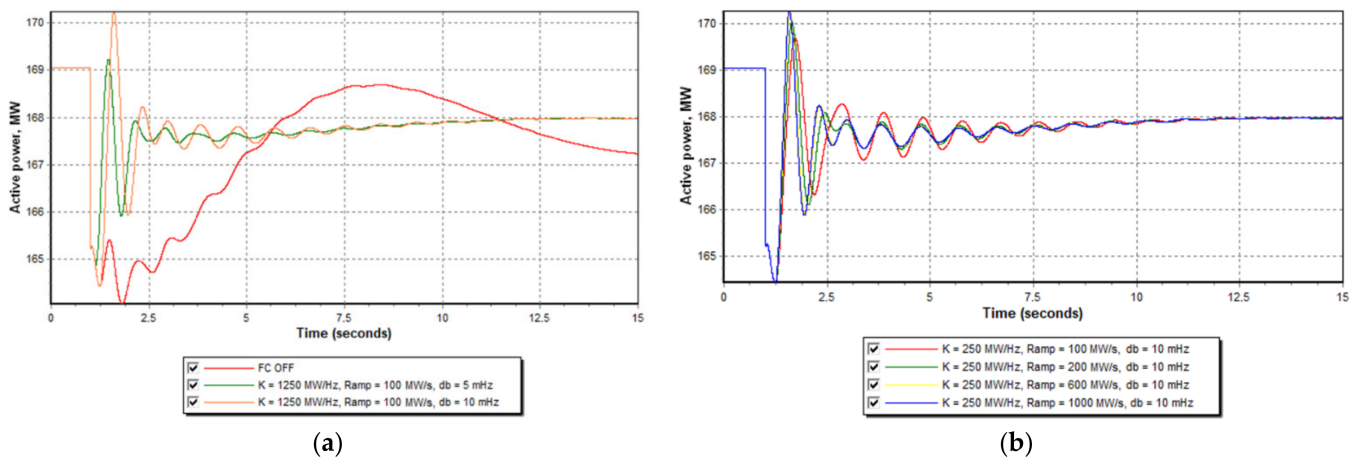
Figure 15. (**a**) Active power compensation of the thermal power plant at different FC parameters. (**b**) Active power compensation of the thermal power plant at different FC parameters.
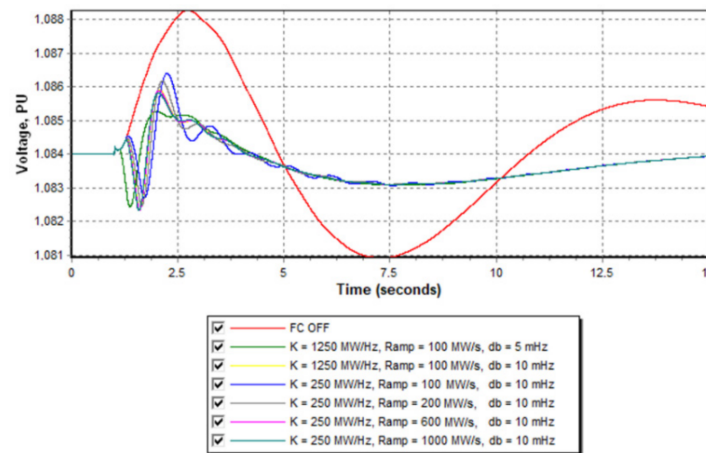
Figure 16. Voltage fluctuations on the 330 kV side.

The results in Figures 13–16 show that both with the gain factor K = 1250 MW/Hz and with K = 250 MW/Hz, damped active power oscillations in the HVDC BtB converter reaction were observed. It is recommended to use a gain of K = 250 MW/Hz during the operation of an isolated EPS.

After SC disconnection, the frequency of the isolated EPS begins to increase. The highest point when the frequency controller is off is 50.08 Hz, and 50.04 Hz when the frequency controller is on [20,22,32,35].

Due to a possible 330 kV voltage spike after disconnecting the SC (synchronous condenser), it is recommended to turn off the SC with reactive power generation Q = 0 MVar [23,36].

5.2. Response of Isolated EPS to SC Disconnection, When 200 MW Generator Has Temporary Droop Settings and Time Constants

A digital simulation was performed with the standard and temporary parameters of the unit operating in generator mode:

Generator temporary droop, r = 1.5;

Turbine regulator temporary time constant, T_r = 10 s.

The generator's standard frequency controller parameters were set as follows:

Gain K = 250 MW/Hz, dead-band = 200 mHz, droop r = 2.5, turbine regulator time constant Tr = 15 s and ramp = 100 MW/s. The simulation results are shown in Figures 17 and 18.

(**a**)

(**b**)
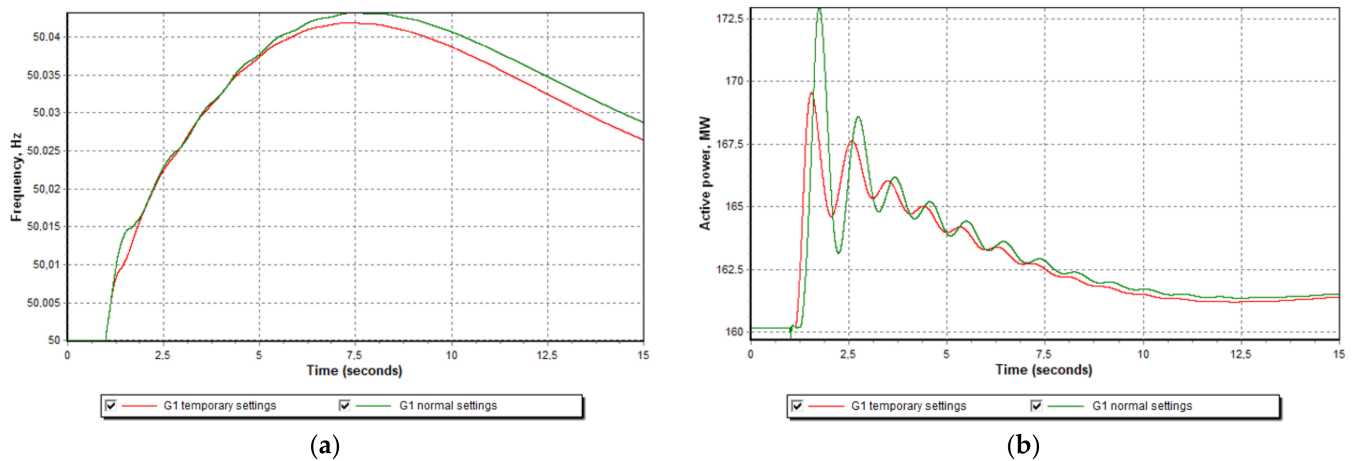
Figure 17. (**a**) Frequency change in the isolated power system in response to SC disconnection. (**b**) Response of the HVDC BtB converter to SC disconnection.
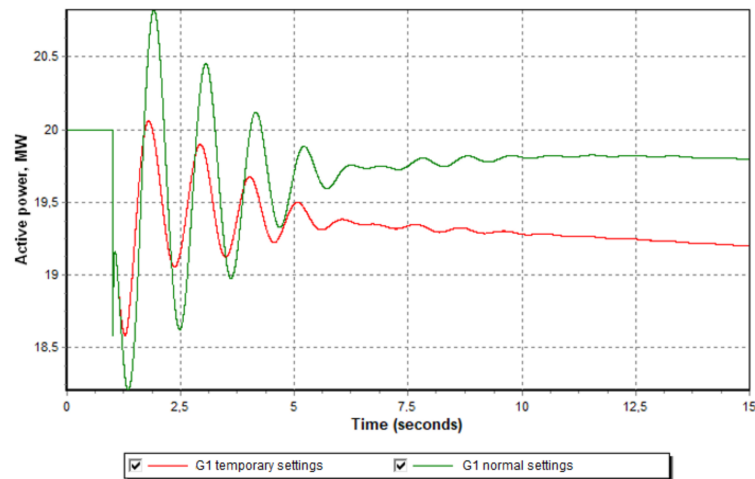
Figure 18. Response of generator (G1) to SC disconnection.

When using the temporary parameters of the unit operating in the generator mode, a smaller frequency increase is seen; in addition, the amplitude of the active power oscillations of the HVDC BtB converter decreases from 10 MW to ~5 MW [20,22,32,35–38].

5.3. Response of Isolated EPS to SC Disconnection, When Two Units Operate in SC Mode

The operation of the isolated EPS must be checked when the HVDC BtB converter is operating in frequency control mode and when oscillations occur. In the isolated EPS, two units are operating in SC (synchronous condenser) mode, when one of them unexpectedly disconnects. The initial conditions for the digital simulation were as follows: 1. HVDC BtB converter frequency controller parameters and gain K = 250 MW/Hz; 2. HVDC BtB converter active power ramp = 100 MW/s. The simulation results are shown in Figure 19.

When two SC units operate and one of them disconnects, a faster dynamic process is observed after the disturbance, i.e., the isolated EPS stabilizes in a shorter period of time, but no significant improvement occurs. It is better to use two units operating in SC mode if possible [20,22,32,35–38].
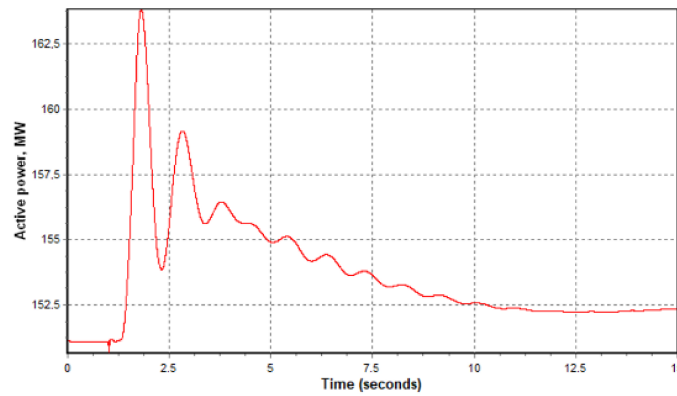
Figure 19. Response of the HVDC BtB converter to SC disconnection.

5.4. Response of Isolated EPS to SC Start-Up

The initial conditions for the digital simulation were as follows:

1. One unit starts operating in synchronous condenser mode;
2. The HVDC BtB converter frequency control gain *K* is 250 MW/Hz and corresponds to 4% droop;
3. The HVDC BtB converter active power ramp speed is 100 MW/s;
4. The HVDC BtB converter dead-band limit of frequency change of the isolated system is 10 mHz.

The simulation results are shown in Figures 20 and 21.

(**a**)

(**b**)
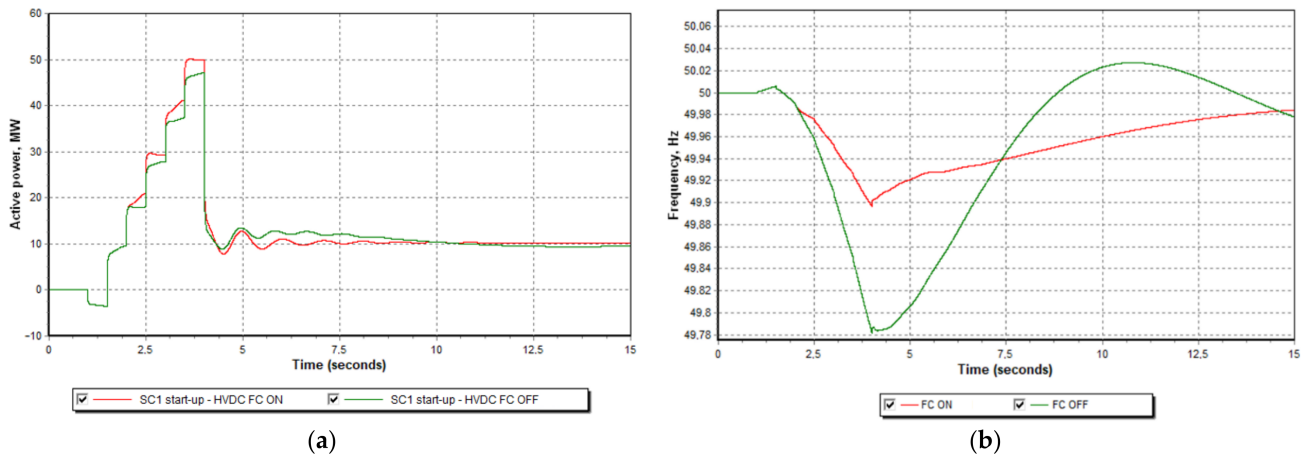
Figure 20. (**a**) Load of SC at start-up. (**b**) Frequency change in the isolated power system.
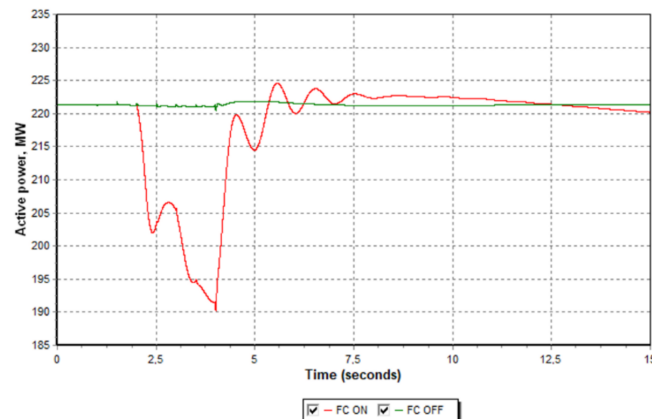
Figure 21. Response of the HVDC BtB converter to SC activation (start-up).

After synchronizing the unit operating in SC mode with the isolated EPS, at the initial point in time, the SC generates electricity to the isolated EPS at about 3 MW (duration 1 s); due to the additional functions required to prepare the unit to operate in SC, demand starts to grow linearly until it reaches a load of (−50 MW), and the length of the process is 10 s. When a load of (−50 MW) is reached, demand spasmodically decreases to (−10 MW) and stabilizes, and the unit can operate indefinitely with a constant demand of (−10 MW). A graphic representation of this process is given in Figure 20a [20,22,32,35–38].

The process of preparing the unit to operate in SC mode causes fluctuations in the frequency of the isolated EPS; if the frequency control function of the HVDC BtB converter is enabled, the frequency of the isolated EPS does not drop below 49.9 Hz. When the frequency control function of the HVDC BtB converter is switched off, the frequency of the isolated EPS drops to 49.78 Hz. The isolated EPS frequency response is shown Figure 20b. The HVDC BtB converter's response to a disturbance is shown in Figure 21 [15,21,22,32].

6. Response of the Isolated System to a Load Change When HVDC BtB Converter's Frequency Control Function Is On

In this section, frequency changes in the islanded system caused by a load increase or decrease while the frequency control capability of the HVDC BtB converter is applied are analyzed. The response of the system is presented when the converter's dead-band setting range is 0 to 200 mHz.

6.1. Response of Isolated EPS to System's Insufficient Frequency, When HVDC BtB Converter's Frequency Control Function Is Enabled

Based on the obtained results, it is assumed in this simulation that the load change soars over 30 MW. The HVDC BtB converter's frequency control gain is $K = 1250$ MW/Hz, and its active power ramp speed is 100 MW/s. The numerical simulation is performed using different dead-bands: 0 mHz, 50 mHz, 100 mHz, 150 mHz, and 200 mHz.

The simulation results are shown in Figures 22 and 23.

Frequency drops using different dead-bands are shown in Table 5. The results obtained show that the frequency control of the HVDC BtB converter reduces the frequency drop. The frequency drop directly depends on the set dead-band. In order to evaluate the frequency control capabilities of the HVDC BtB converter, the use of a 0 mHz dead-band is not recommended during the operation of an isolated EPS [15,21,22,32].

(a) (b)
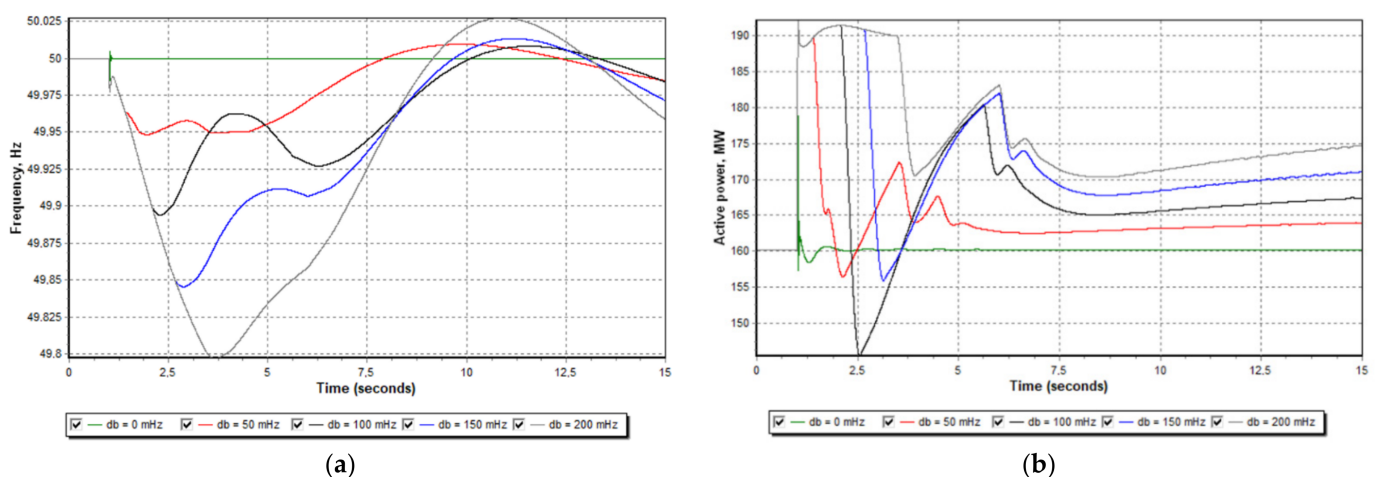
Figure 22. (**a**) Frequency change when the HVDC BtB converter has a different frequency insensitivity range. (**b**) Response of the active power of the HVDC BtB converter to insufficient frequency.
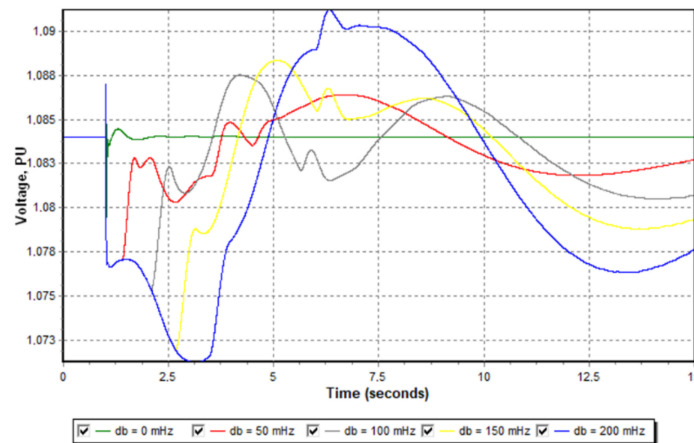
Figure 23. Voltage fluctuations on the 330 kV side.

Table 5. Frequency change in the isolated power system.

Frequency Insensitivity Range of HVDC BtB Converter, mHz	Frequency, Hz
0	49.98
50	49.95
100	49.89
150	49.84
200	49.79

The smallest frequency drop occurs when using the HVDC BtB converter dead-bands of 0–50 mHz. If possible, use a 0 mHz HVDC BtB converter dead-band.

6.2. Response of Isolated EPS to Load Reduction, When HVDC BtB Converter Frequency Control Function Is Enabled

In the numerical simulation, it is assumed that the load change soars over 30 MW. The frequency control gain *K* of the HVDC BtB converter is 1250 MW/Hz. The active power ramp speed is 100 MW/s. The digital simulation is performed by setting different HVDC BtB converter frequency dead-bands: 0 mHz, 50 mHz, 100 mHz, 150 mHz, and 200 mHz. The simulation results are shown in Figures 24 and 25.

(**a**)

(**b**)
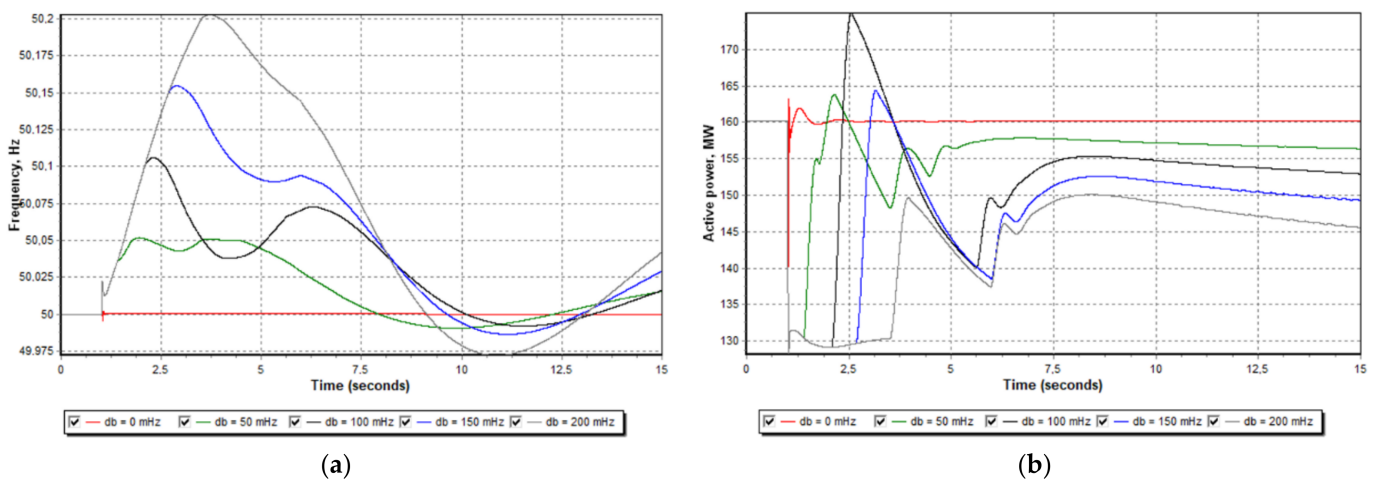
Figure 24. (**a**) Frequency change when the HVDC BtB converter has a different frequency insensitivity range. (**b**) Response of the active power of the HVDC BtB converter to excess frequency.
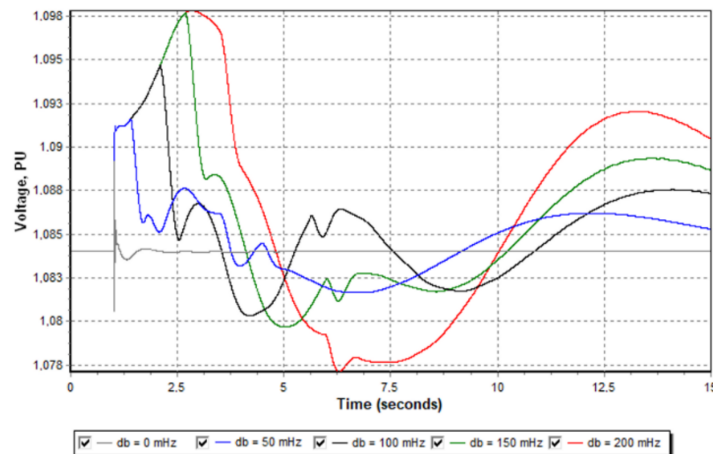
Figure 25. Voltage fluctuations on the 330 kV side.

Frequency increases using different dead-bands are shown in Table 6. The obtained results show that the frequency control of the HVDC BtB converter reduces the frequency drop. The frequency change directly depends on the set dead-band. In order to evaluate the frequency control capabilities of the HVDC BtB converter, the use of a 0 mHz dead-band is not recommended during the operation of an isolated EPS [15,21,22,32].

Table 6. Frequency increase in the isolated power system.

Frequency Insensitivity Range of HVDC BtB Converter, mHz	Frequency, Hz
0	50.00
50	50.05
100	50.11
150	50.16
200	50.21

The smallest frequency increase occurs when using the HVDC BtB converter dead-bands of 0–50 mHz. If possible, use a 0 mHz HVDC BtB converter dead-band.

Isolated EPS voltage stability problems occur when the HVDC BtB converter dead-band is greater than 100 mHz. The voltage of 330 kV in the isolated EPS during the active power spike exceeds the permissible (362 kV) limit by 1.097 [16–19,24]. A decrease in load causes an increase in voltage.

7. Analysis of the System's Emergency Modes

The capability of the isolated system to withstand disconnection of the unit operating in pump mode and the HVDC BtB converter's disconnection during emergency cases is analyzed in this section. The impact of the HVDC BtB converter's frequency control function during disconnection of the unit operating in pump mode is considered.

7.1. Emergency Operating Mode of Isolated EPS When Disconnection of Unit Operating in Pump Regime Is Necessary

In the numerical simulation, the disconnection of the unit operating in a pump mode is analyzed. In order to minimize the impact on the isolated EPS, the system demand must be reduced to 110 MW before disconnecting the pump from the mains. The simulation was performed for two cases: 1. The frequency control function in the HVDC BtB converter was activated; 2. The frequency control function in the HVDC BtB converter was deactivated.

The HVDC BtB converter frequency control parameters were as follows: the gain K was 250 MW/Hz and corresponded to 4% droop; active power ramp speed was 100 MW/s; dead-band was 10 mHz. The simulation results are shown in Figure 26a,b.

(**a**)

(**b**)
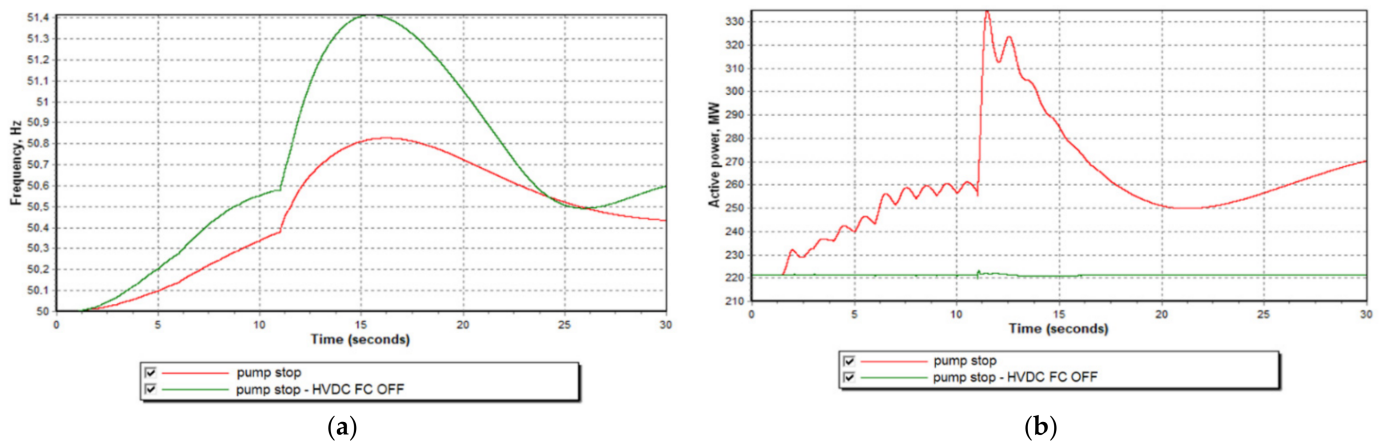
Figure 26. (**a**) Frequency change in the isolated power system caused by disconnection of the unit operating in pump mode. (**b**) Response of the HVDC BtB converter to a disconnection of the unit operating in pump mode.

A significantly greater, instantaneous frequency increase is seen when the frequency control function in the HVDC BtB converter is switched off; in this case, the frequency instantaneously increases to 51.4 Hz. When the frequency control mode is activated in the HVDC BtB converter and the frequency control capabilities are assumed to be ± 100 MW, the frequency increase stops at the limit of 50.82 Hz [15,21,22,32]. In both cases, the isolated EPS does not reach the maximum permissible frequency limit of 51.5 Hz [16–19,24].

7.2. System Emergency Mode—HVDC BtB Converter Disconnection

During the numerical simulation, a disconnection of the HVDC BtB converter is analyzed. The maximum power ramp speed of the HVDC BtB converter is 15 MW/s. The transmitted power of the HVDC BtB converter was reduced to 50 MW (minimum power that can be transmitted), and only then was the converter disconnected. The simulation results are shown in Figure 27.
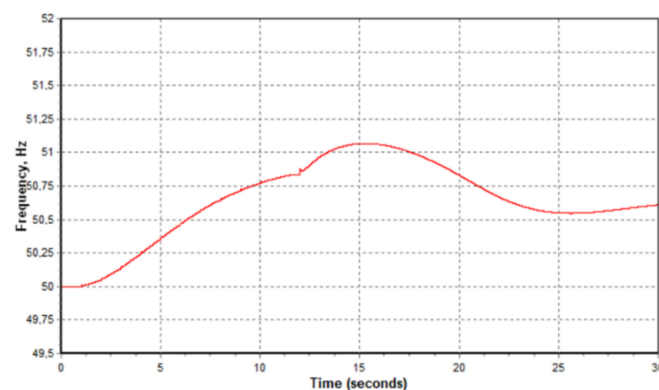
Figure 27. Frequency change in the isolated power system caused by disconnection of the HVDC BtB converter.

If it is necessary to disconnect the HVDC BtB converter when the active power is reduced at a ramp of 15 MW/s, an instantaneous frequency increase to 51.1 Hz is observed, but the isolated EPS remains stable.

8. Conclusions

Stability-related questions regarding the electric power system (EPS) operating in an islanded mode were addressed in this research. The considered issues include: the reaction of the islanded system to a load change with and without the HVDC BtB con-

verter's frequency control capabilities; switching on/off the units working in synchronous condenser mode; the optimization of the HVDC BtB converter's settings and the reaction of the system to major disturbances, such as the disconnection of the pumped-storage power station's unit working in pump mode and the disconnection of the HVDC BtB converter. The summarized results of the research are:

In the isolated EPS, a 200 mHz frequency deviation is reached in the case of a 25 MW disturbance after disabling the HVDC BtB converter frequency control function.

It is recommended to use two switched-on harmonic filters of the HVDC BtB converter during the operation of the isolated EPS.

The optimal HVDC BtB converter frequency control parameters during simulation are as follows: gain factor K = 250 MW/Hz, corresponding to 4% droop; ramp = 100 MW/s; dead-band db = 10 mHz; control range $\pm$50 MW.

When two synchronous condenser units are operating and one of them disconnects, a faster dynamic process is observed after the disturbance, i.e., the isolated EPS stabilizes in a shorter period of time. If possible, it is recommended to use two units operating in synchronous condenser mode.

Connecting a synchronous condenser unit to the isolated EPS results in a system frequency reduction of up to 200 mHz when the frequency control function of the HVDC BtB converter is switched off, and 100 mHz when the frequency control function of the HVDC BtB converter is switched on.

In the isolated EPS, short-term overvoltage up to 363 kV is possible when the HVDC BtB converter operates in frequency control mode. In response to the frequency increase, it is recommended that the voltage of the isolated EPS not exceed 357 kV before switching on the frequency control function of the HVDC BtB converter.

Author Contributions: Conceptualization, R.D.; methodology, R.L.; software, K.O.; validation, R.L.; formal analysis, R.D.; investigation, K.O. and R.L.; resources, R.L.; data curation, R.D.; writing—original draft preparation, K.O., R.D. and R.L.; writing—review and editing, K.O., R.D. and R.L.; visualization, R.L.; supervision, R.D. All authors have read and agreed to the published version of the manuscript.

References

1. Del Rosso, A.D.; Anello, M.; Spittle, E. Stability assessment of isolated power systems with large induction motor drives. In Proceedings of the IEEE/PES Transmission & Distribution Conference and Exposition, Caracas, Venezuela, 15–18 August 2006. [CrossRef]
2. Yu, Y.N. *Electric Power System Dynamics*; Academic Press: New York, NY, USA, 1983; pp. 25–143.
3. Sauer, P.W.; Pai, M.A. *Power System Dynamics and Stability*; Prentice Hall Press: Hoboken, NJ, USA, 1998; pp. 19–98.
4. Dysko, A.; Leithead, W.E.; O'Reilly, J. Enhanced power system stability by coordinated PSS design. *IEEE Trans. Power Syst.* **2010**, *25*, 413–422. [CrossRef]
5. Kundur, P. *Power System Stability and Control*; McGraw Hill Press: New York, NY, USA, 1994.
6. Kamwa, I.; Grondin, R.; Trudel, G. IEEE PSS2B versus PSS4B: The limits of performance of modern power system stabilizers. *IEEE Trans. Power Syst.* **2005**, *20*, 903–915. [CrossRef]
7. Boukarim, G.E.; Wang, S.; Chow, J.H.; Taranto, G.N.; Martins, N. A comparison of classical robust and decentralized designs for multiple power system stabilizers. *IEEE Trans. Power Syst.* **2000**, *15*, 1287–1292. [CrossRef]
8. Kundur, P.; Paserba, J.; Ajjarapu, V.; Andersson, G.; Bose, A.; Canizares, C. Definition and classification of power system stability. *IEEE Trans. Power Syst.* **2004**, *19*, 1387–1401. [CrossRef]
9. Pai, M.A. *Energy Function Analysis for Power System Stability*; Springer Press: Berlin, Germany, 2012.
10. Ruiz-Vega, D.; Pavella, M. A comprehensive approach to transient stability control. I. Near optimal preventive control. *IEEE Trans. Power Syst.* **2003**, *18*, 1446–1453. [CrossRef]
11. Chiang, H.D. *Direct Methods for Stability Analysis of Electric Power Systems*; Wiley Press: New York, NY, USA, 2011.
12. Machowski, J.; Bialek, J.W.; Bumby, J.R. *Power System Dynamics: Stability and Control*, 2nd ed.; Wiley Press: Chichester, UK, 2008.
13. Dondi, P.; Bayoumi, D.; Julian, D.; Haederli, C.; Suter, M. Network integration of distributed power generation. *J. Power Sources* **2002**, *106*, 1–9. [CrossRef]

14. Ritonja, J.; Petrun, M.; Cernelic, J.; Brezovnik, R.; Polajzer, B. Analysis and applicability of Heffron–Phillips model. *Elektron. Elektrotech.* **2016**, *22*, 3–10. [CrossRef]

15. Tamrakar, U.; Shrestha, D.; Malla, N.; Ni, Z.; Hansen, T.M.; Tamrakar, I.; Tonkoski, R. Comparative analysis of current control techniques to support virtual inertia applications. *Appl. Sci.* **2018**, *8*, 2695. [CrossRef]

16. Vidal-Clos, J.A.; Bullich-Massagué, E.; Aragüés-Peñalba, M.; Vinyals-Canal, G.; Chillón-Antón, C.; Prieto-Araujo, E.; Gomis-Bellmunt, O.; Galceran-Arellano, S. Optimal operation of isolated microgrids considering frequency constraints. *Appl. Sci.* **2019**, *9*, 223. [CrossRef]

17. Zhang, N.; Zhou, Q.; Hu, H. Minimum frequency and voltage stability constrained unit commitment for AC/DC transmission systems. *Appl. Sci.* **2019**, *9*, 3412. [CrossRef]

18. European Union. Establishing a network code on electricity emergency and restoration. Commission regulation (EU) 2017/2196 of 24 November 2017. *Off. J. Eur. Union* **2017**, *L312*, 54–85.

19. European Union. Establishing a guideline on electricity transmission system operation. Commission regulation (EU) 2017/1485 of 2 August 2017. *Off. J. Eur. Union* **2017**, *L220*, 1–120.

20. Dudgeon, G.J.W.; Leithead, W.E.; Dysko, A.; O'Reilly, J.; McDonald, J.R. The effective role of AVR and PSS in power systems: Frequency response analysis. *IEEE Trans. Power Syst.* **2007**, *22*, 1986–1994. [CrossRef]

21. Elices, A.; Rouco, L.; Bourles, H.; Margotin, T. Design of robust controllers for damping interarea oscillations: Application to the European power system. *IEEE Trans. Power Syst.* **2004**, *19*, 1058–1067. [CrossRef]

22. Moulin, L.S.; Da Silva, A.A.; El-Sharkawi, M.; Marks, R.J. Support vector machines for transient stability analysis of large-scale power systems. *IEEE Trans. Power Syst.* **2004**, *19*, 818–825. [CrossRef]

23. Rajapakse, A.D.; Gomez, F.; Nanayakkara, K.; Crossley, P.A.; Terzija, V.V. Rotor angle instability prediction using post-disturbance voltage trajectories. *IEEE Trans. Power Syst.* **2010**, *25*, 947–956. [CrossRef]

24. Mohammadi, F.; Nazri, G.A.; Saif, M. An improved mixed AC/DC power flow algorithm in hybrid AC/DC grids with MT-HVDC systems. *Appl. Sci.* **2020**, *10*, 297. [CrossRef]

25. Tina, G.M.; Maione, G.; Licciardello, S.; Stefanelli, D. Comparative technical-economical analysis of transient stability improvements in a power system. *Appl. Sci.* **2021**, *11*, 11359. [CrossRef]

26. Stefanov, P.C.; Stankovic, A.M. Modeling of UPFC operation under unbalanced conditions with dynamic phasors. *IEEE Trans. Power Syst.* **2002**, *17*, 395–403. [CrossRef]

27. Wall, P.; Gonzalez-Longatt, F.; Terzija, V. Demonstration of an inertia constant estimation method through simulation. In Proceedings of the 45th International Universities Power Engineering Conference (UPEC), Cardiff, UK, 31 August–3 September 2010.

28. Alinejad, B.; Kazemi Karegar, H. Online inertia constant and Thévenin equivalent estimation using PMU data. *Int. J. Smart Electr. Eng.* **2014**, *3*, 73–78.

29. Inoue, T.; Taniguchi, H.; Ikeguchi, Y.; Yoshida, K. Estimation of power system inertia constant and capacity of spinning-reserve support generators using measure frequency transients. *IEEE Trans. Power Syst.* **1997**, *12*, 136–143. [CrossRef]

30. Wang, Y.; Silva-Saravia, H.; Pulgar-Painemal, H. Estimating inertia distribution to enhance power system dynamics. In Proceedings of the North American Power Symposium (NAPS), Morgantown, WV, USA, 17–19 September 2017. [CrossRef]

31. Gibbard, M.J.; Martins, N.; Sanchez-Gasca, J.J.; Uchida, N.; Vital, V.; Wang, L. Recent applications of linear analysis techniques. *IEEE Trans. Power Syst.* **2001**, *16*, 154–162. [CrossRef]

32. Gibbard, M.J.; Vowles, D.J. Reconciliation of methods of compensation for PSSs in multimachine systems. *IEEE Trans. Power Syst.* **2004**, *19*, 463–472. [CrossRef]

33. Zhang, X.P.; Handschin, E.; Yao, M. Modeling of the generalized unified power flow controller (GUPFC) in a nonlinear interior point OPF. *IEEE Trans. Power Syst.* **2001**, *16*, 367–373. [CrossRef]

34. Ji, L.; Wu, J.; Zhou, Y.; Hao, L. Using trajectory clusters to define the most relevant features for transient stability prediction based on machine learning method. *Energies* **2016**, *9*, 898. [CrossRef]

35. Vaccaro, A.; Canizares, C.A. A knowledge-based framework for power flow and optimal power flow analyses. *IEEE Trans. Smart Grid* **2018**, *9*, 230–239. [CrossRef]

36. Gurrala, G.; Dinesha, D.; Dimitrovski, A.; Simunovic, S.; Pannala, S.; Starke, M. Large multi-machine power system simulations using multi-stage adomian decomposition. *IEEE Trans. Power Syst.* **2017**, *32*, 3594–3606. [CrossRef]

37. Ritonja, J.; Polajžer, B. Analysis of synchronous generators' local mode eigenvalues in modern power systems. *Appl. Sci.* **2022**, *12*, 195. [CrossRef]

38. Verdejo, H.; Moreira, P.; Kliemann, W.; Becker, C.; Delpiano, J. An analytical model for small signal stability analysis in unbalanced electrical power systems. *Appl. Sci.* **2020**, *10*, 8855. [CrossRef]